Study of the entrainment in the Saharan Boundary Layer based on observations and Large Eddy Simulations

G. Canut, F. Couvreux, M. Lothon, D. Pino, F. Saïd

1. Introduction

In the presence of windshear, the entrainment process is still not correctly represented in various models. This article is devoted to the study of the entrainment at the interface between the moist and cold monsoon flow and the dry and warm Saharan Air Layer (SAL) which gives very specific conditions where the Planetary Boundary Layer (PBL) grows within the monsoon flow and rapidly reaches the bottom of the SAL (see Canut et al. (2010)), leading to a large windshear and large thermodynamical differences at the top.

We took advantage of a statistical study based on the measurements made by the French ATR aircraft during the AMMA (African Monsoon Multidisciplinary Analysis) experiment, which has shown the presence of 'dry tongues' i.e intrusions of dry air from the SAL into the PBL. Those are full part of the entrainment process at the PBL top and responsible for large moisture fluxes in the upper PBL, due to the large difference in humidity between the SAL and the PBL. The study showed a particularly thick entrainment zone in this region during the observation period.

Observations and some numerical simulations based on Large Eddy Simulation (LES) are used in order to better understand the physical processes.

A first LES simulation was designed based on the observations of the 5 June 2006, a case under significant monsoon windspeed during the transition period from the dry season to the active monsoon months. This numerical model resolves the large eddies contributing to the entrainment.

For this day, a complete set of observations was obtained (Canut et al. (2010)) in the area of Niamey (Niger, 13.5° N 2.1° E) with 4 radiosoundings, a wind profiler, ground stations and an aircraft, which flew vertical soundings and several stacked legs. This day of dry convection was chosen because: a convective boundary layer developed without cloud development and the entrainment process was important. The vertical profile of the buoyancy and humidity fluxes were linear, and allowed us to estimate the entrainment rate. The humidity flux at the PBL top was important ($700\ W\ m^{-2}$) whereas it was very small at the ground.

In a second step, a set of 8 sensitivity tests was made with a large range of thermo-dynamic gradient and windshear between the PBL and the free atmosphere in order to evaluate the effect of the windshear on the entrainment processes and to evaluate the different entrainment parameterizations in realistic conditions. In the literature, the authors often use an approach with idealised conditions.

A mixed-layer approach is finally used to further understand the boundary layer characteristics. Two types of mixed layer models have been used. The main difference leans on the characterization of the entrainment zone depth (Fig. 1). The most basic approach, first proposed by Lilly (1968), represents the entrainment zone as a sharp discontinuous inversion ($\delta = 0$), namely, a zero-order-jump model (ZOM). From the 1970s onward, and with different degrees of complexity, this approach has been widely applied to study the CBL over land (e.g. Tennekes (1973); Stull (1976)), the stratocumulus-topped boundary layer, the forma-

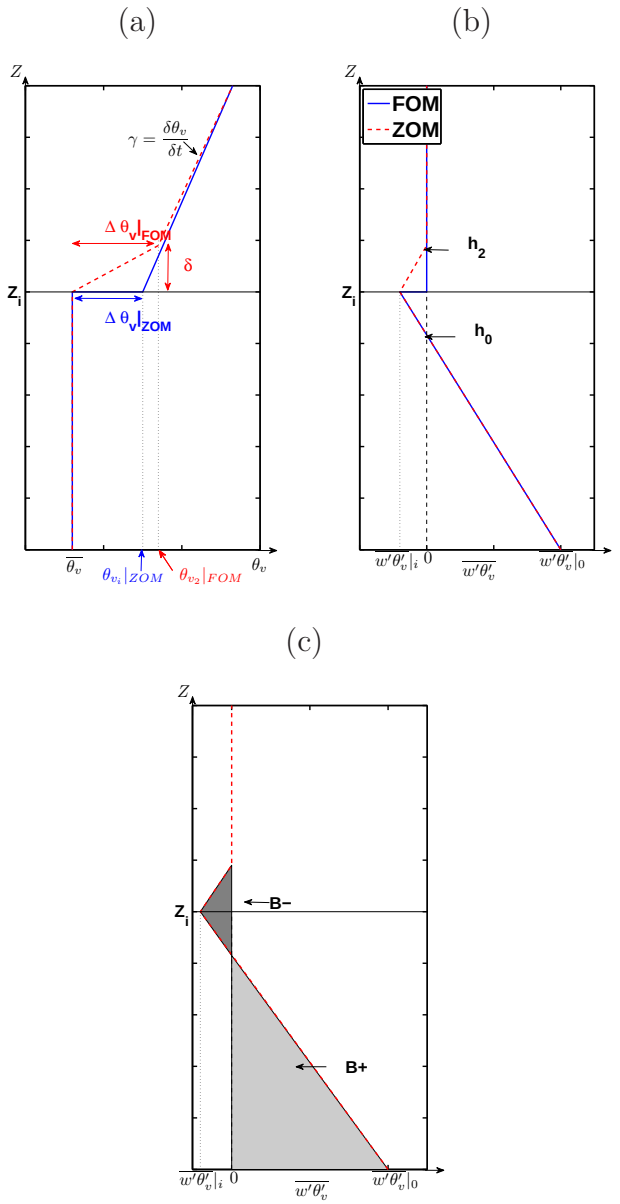

FIG. 1. *Vertical profiles of (a) the virtual potential temperature and (b) the buoyancy flux assumed in (blue) zero-order-jump model (ZOM) and (red) a first-order-jump model (FOM). (c) The sign of the buoyancy flux defines two surfaces B- and B+, obtained by integrating the flux with the height.*

tion of a coastal internal boundary layer, the marine boundary layer, and the impact of boundary layer dynamics on the carbon dioxide concentration or on the atmospheric chemistry in the CBL.

The interface layer can also be described in a more realistic way by the so-called first-order-jump model (FOM). The entrainment region is then assumed to have a finite thickness ($\delta > 0$). In this model (Betts (1974); Sullivan et al. (1998); Van Zanten et al. (1999)), the estimation of the thickness of the entrainment zone is a key parameter.

2. Numerical setup

a. The characteristics of the LES model

The model used in this study is the LES version of the non-hydrostatic model Meso-NH, the dynamical part of which was presented by Lafore et al. (1998). The 3-D turbulence scheme is based on that proposed by Redelsperger and Sommeria (1982) and was discussed in details by Cuxart et al. (2000). It is based on a prognostic equation for subgrid kinetic energy and it incorporates the effect of thermal stratification on subgrid fluxes through varying Prandtl and Schmidt numbers. This model enables to analyse the structure and the evolution of the boundary layer.

A 10 km × 10 km × 5 km domain was used, centred over Niamey. The setup of the simulation was very similar to that of Couvreux et al. (2005) for an IHOP case. The horizontal resolution was 100 m and we considered a flat domain which characterizes the region. The same vertical profile was used as initialisation on the whole horizontal domain. A vertical stretched grid of 60 levels was used with resolution thinner than 50 m up to 1000 m, and 100 m higher up. The lateral conditions were cyclic and the duration of the simulation was 12 h. At the surface, the heat fluxes were prescribed. At the domain top, in order to avoid the reflection of gravity waves, an absorbant layer of 1 km was added, where the fields were nudged towards the mean profiles. Large-scale advections of

heat and moisture have been taken into account, since observations indicated that they were not negligible during the observing period.

b. The initial conditions

Several sensitivity tests on the initial conditions allowed us to define the final configuration for the simulation of 5 June 2006. In this simulation, different forcings have been introduced to obtain a simulation with a vertical structure close to the observations. Initial profiles and large scale advections (prescribed every 3 hours) were deduced from the ECMWF reanalyses (Agusti-Panareda et al. (2010)). No advection was prescribed above the PBL top. The surface sensible heat flux varied during the day with a maximum at midday of 400 W m^{-2} consistent with observations from the Atmospheric Radiation Measurement (ARM) mobile facility. During the pre-onset period that is a moistening period before the most active phase of the monsoon, the surface latent heat flux was very small and we chose to neglect it.

c. Validation of the simulation

The validation of the LES has been possible thanks to the numerous observations made during this day. Figure 2 shows the water vapour mixing ratio (r_v), potential temperature (θ) and zonal wind component (U) vertical profiles by the LES and observations at midday. For θ, r_v and U the different jumps at the PBL top are well predicted (4 K, 5 g kg $^{-1}$ and 9 m s^{-1} respectively). The variability found with the observations is also reproduced in the LES. For the meridian wind component (V) differences between observations and LES are observed (figure 2d).

The evolution of the PBL top is a crucial parameter because the determination of the entrainment processes greatly depends on it. Figure 3 compares 4 different methods to obtain the PBL depth by using LES against the observations (wind profiler and soundings). In those 4 methods the PBL top is defined as: (i) the height of the mini-

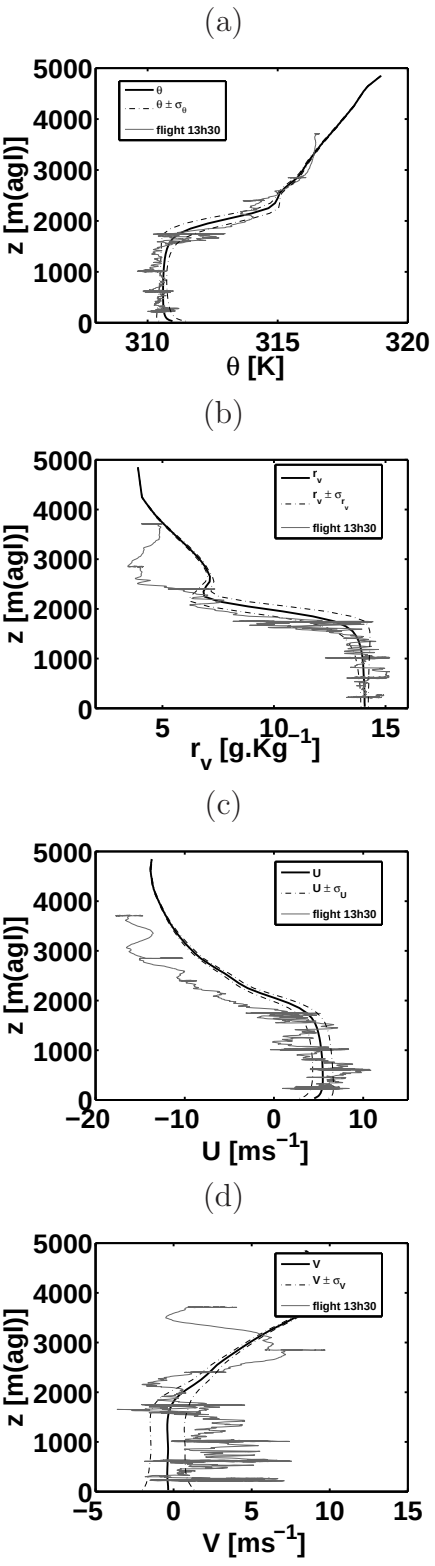

FIG. 2. *(solid) Simulated between 13 and 14h, and (grey) observed during the flight around 13h30, vertical profiles of (a) θ, (b) r_v, (c) zonal and (d) meridian wind component. The dashed lines represent the variability in the model domain.*

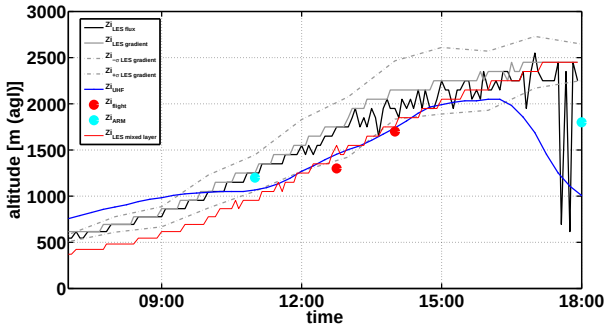

FIG. 3. *Temporal evolution of the PBL height obtained on 5 June 2006 with (blue dots) the radiosoundings of the ARM station, (red dots) the aircraft observations and (blue line) the wind profiler observations at Niamey every 15 minutes. In the LES the PBL height was obtained with (red line) the top of the mixed layer method, (black line) the buoyancy flux method, (dark grey lines) the method of the maximum of gradient, (dashed grey line) variability with the gradient method .*

mum buoyancy flux (LES), (ii) the height of maximum gradient of potential temperature (LES), (iii) the top of the mixed layer (flight observations, radiosoundings and LES), (iv) the height of maximum radar refectivity (wind profiler). As expected the mixed layer top is found below the maximum gradient of the potential temperature (Sullivan et al. (1998)).

When the same mixed layer method is used, PBL top obtained by LES fits well the observations. The wind profiler data allow us to confirm the rapid evolution of the PBL between 10 and 15 h. Considering all the available data, we estimated the PBL growth rate around 10 cm s $^{-1}$.

In this work, we used the level of the mixed layer top in the LES to compare with the observations while the most frequently for LES estimations is the level of minimun buoyancy flux.

3. Impact of entrainment of dry air on the PBL structure

In order to study the entrainment process we used the fluctuations measured by aircraft and calculated by LES. For example, the vertical velocity can be written:

$$w = \overline{w} + w' \tag{1}$$

where w is the measured vertical velocity, $\overline{w}$ is the mean during a given period and w' is the fluctuation. The same equation is used for potential temperature (θ), virtual potential temperature (θ_v) and water vapour mixing ratio (r_v).

LES and aircraft observations provide information about the structure of the PBL, and the role of the dry tongues. During this period, due to the almost quasi-zero latent heat fluxes, the main source of the humidity variability in the PBL is the entrained dry air from the free troposphere into the PBL. Analysis of the fluctuations in potential temperature, water vapour mixing ratio and vertical velocity, both with the observations and LES, highlights the presence of dry intrusions at the PBL top which penetrate down to the middle of the PBL, and even lower (Lohou et al. (2010)). Dry tongues participate to the vertical redistribution of the water vapour and other scalars. Close to the PBL top, they have a typical width of 500 m and a distance between them of 2 km (Canut et al. (2010)).

Variances and fluxes result from the impact of these dry tongues. Figures 4 and 5 show the variances and the flux vertical profiles for the observations and the LES.

For this day, we observed an overestimation of the surface buoyancy heat flux by the LES. For the humidity flux the large value at the PBL top was well represented by the LES. This large value is due to negative fluctuations of vertical velocity and water vapour mixing ratio at the top which correspond to the exchanges between dry SAL and moist PBL.

The vertical profiles of water vapour mixing ratio and buoyancy fluxes observed this day are close to linear in the PBL. This allows us to estimate the entrainment rate defined as:

$$\beta = -\frac{\overline{w'\theta'_v}|_i}{\overline{w'\theta'_v}|_0}. \tag{2}$$

where $\overline{w'\theta'_v}|_i$ and $\overline{w'\theta'_v}|_0$ are the buoyancy fluxes at the PBL top and at the surface respectively.

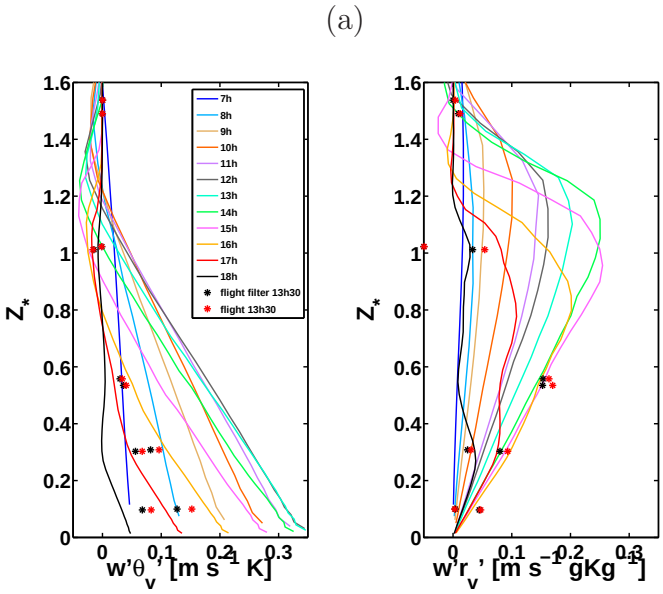

FIG. 4. *Temporal evolution of the simulated vertical profiles of (a) the buoyancy flux and (b) the moisture flux (hourly averaged in all the domain). $*$ represent the observed flux obtained (red) after filtering the data with a 5 km cut off wavelength and (black) with no filtering. Z_* represents the height normalized by the PBL top.*

We found an entrainment rate close to 0.3 with the observations around 13h30, larger than the typical 0.2 value found for purely convective PBL (Garratt (1992)). With the LES, the entrainment rate increased during the day but remained smaller than 0.2. Figure 5 shows the variances of θ, r_v and w. In the entrainment zone retrieved by the LES, the maxima of the potential temperature and of the water vapour mixing ratio variance were very large. The few observed points in this layer do not allow a complete comparison with the LES data. Note that Turner et al. (2010) observed the same order of magnitude with Raman lidar. These profiles are due to strong exchanges between the PBL and the free troposphere characteristic for a convective boundary layer. At the surface, both the simulation and the observations show small values in the water vapour mixing ratio variance.

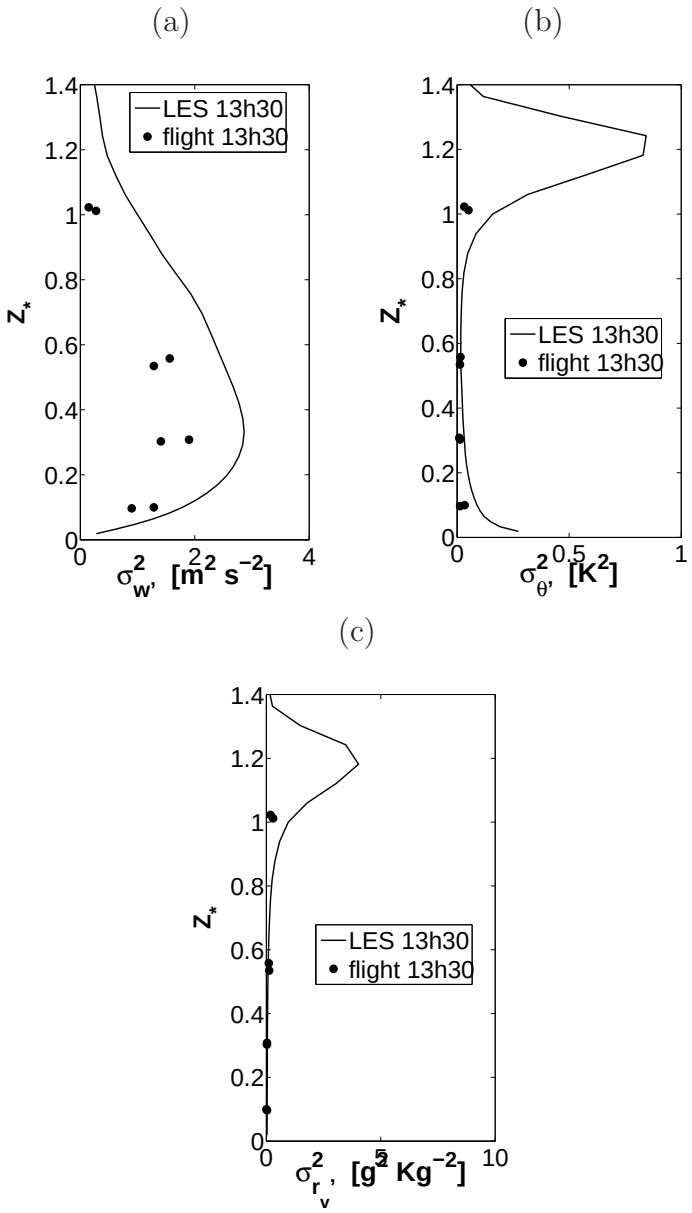

FIG. 5. *Vertical profiles of the (line) simulated and (dots) observed variance of (a) vertical velocity, (b) water vapour mixing ratio and (c) potential temperature for 5 June 2006.*

The water vapour mixing ratio fluctuations within the PBL are only generated in the entrainment zone. On contrary the potential temperature fluctuations are generated both at the surface and at the entrainment zone. As a consequence, the potential temperature variance is important at the surface for the simulation and for the observa-

tions but it is over-estimated by the simulation. LES also overestimates the vertical velocity variance in the middle of the PBL. The observations show a similar profile with a maximum at 600 m (0.3 Z_i) but the variance is 2 times larger in the simulation. This presently remains unexplained and implies that the w - r_v correlation coefficients are underestimated by the LES since the moisture fluxes are similar.

In order to estimate the contribution of dry tongues to the variances and fluxes relative to the contribution of thermals, a conditional analysis on the fluctuations w', θ' and r'_v (Grossman and Nimal (1995)) is used. We defined three classes: thermals with $w' > 0$ and $\theta' > 0$, dry tongues with $w' < 0$, $r'_v < 0$ and $\theta' > 0$, and the remaining population in the third class.

With this conditional sampling (Fig. 6), the simulation fits very well aircraft observations. The conditional sampling of the fluctuations revealed that the dry tongues are not necessarily the most numerous turbulent structures, but that they contribute 40% to the variance of water vapour mixing ratio in the upper part of the PBL. In the middle of the PBL, they participate to between 20 and 40% to the variance of the potential temperature. Close to half of the most intense fluctuations in vertical velocity ($< -\sigma_{w'}$) at the PBL top are associated with positive fluctuations of potential temperature and negative fluctuations of water vapour mixing ratio. The dry tongues generate intense fluctuations, consistently with observations by Couvreux et al. (2007) and Canut et al. (2010).

The analysis of the distributions has been carried out (not shown). In the middle of the PBL, LES represented correctly the distributions observed for the 3 variables. At the interfaces surface/PBL and PBL/free atmosphere, we found more differences between observations and LES, similary to the previous comparison of variances. Again, we impute it to a sampling problem and cannot conclude in any overestimation by the LES.

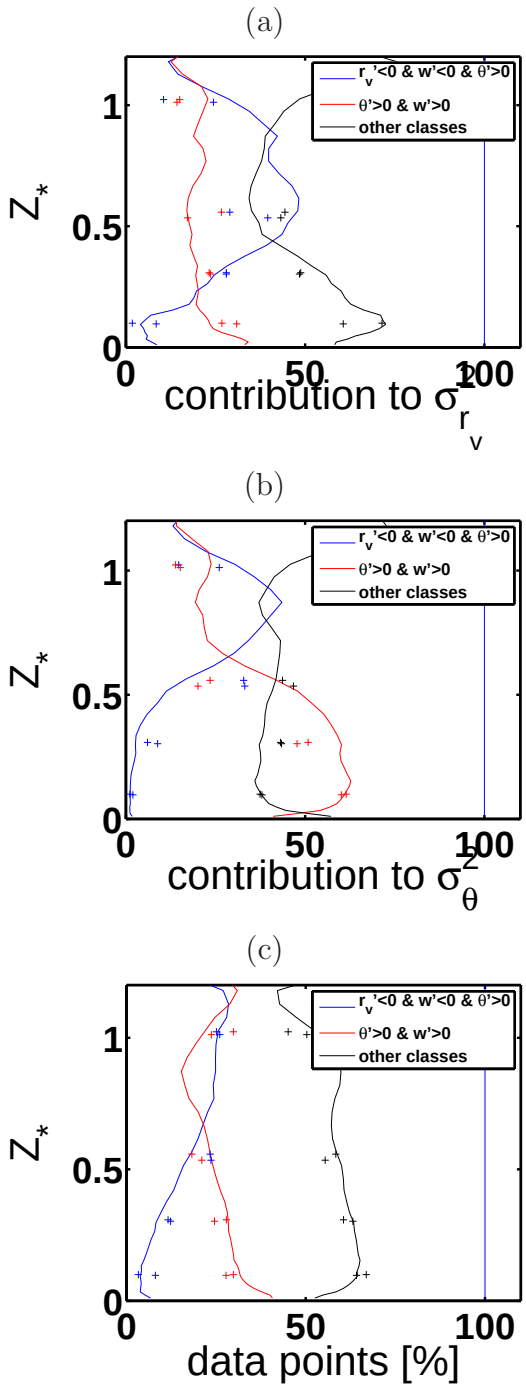

FIG. 6. *Contribution of the different classes at 14h to (a) humidity variance, (b) potential temperature variance. (c) Distribution of data points over the different classes according to (solid line) LES and (crosses) aircraft observations for 5 June 2006.*

4. Test of some parameterisations of entrainment with a sensitivity study

To improve our understanding of the entrain-

ment processes within the Sahelian boundary layer and in particular during the gradually moistening period before the full monsoon, several tests of sensitivity (table 1) are made with a reference simulation which corresponds to the case of 5 June 2006 previously described .

nom	Z_i	adv	θ_0	$\frac{\delta\theta}{\delta z}$	$\frac{\delta r_v}{\delta z}$	ws_{max}
run02	500	$\neq 0$	303.0	11.9	-5.4	12.0
run03	500	0	303.0	11.9	-5.4	12.0
test44	0	0	304.5	5.0	-3.2	12.0
test48	0	0	299.0	7.7	-5.5	12.0
test49	300	0	303.2	26.1	-16.7	12.0
test45	500	0	303.0	11.9	-5.4	7.0
test46	500	0	303.0	11.9	-5.4	6.0
test47	500	0	303.0	11.9	-5.4	3.0

TABLE 1. *Initial conditions at 6h: Z_i $[m]$: height of the PBL; adv: large scale advection; θ_0 $[K]$: θ at the surface; $\frac{\delta\theta}{\delta z}$ $[10^{-3}K.m^{-1}]$: in the entrainment zone or in the PBL in the cases without PBL developped; $\frac{\delta r_v}{\delta z}$ $[10^{-3}g\ kg^{-1}\ m^{-1}]$: in the entrainment zone or in the PBL in the cases without developped PBL; ws_{max} $[m.s^{-1}]$ represents the maximum of windshear. The test called run02 represents the simulation on 5 June 2006 and the test called run03 is the reference test without advection.*

For the different tests no large scale advection is prescribed and an homogeneous surface flux with a maximum of 400 W m^{-2} is used. Only the initial vertical profiles of potential temperature, water vapour mixing ratio and wind, vary over a range covering the conditions observed during the pre-onset period.

Figure 7 shows the different initial profiles used which correspond to realistic but simplified profiles observed during the pre-onset period. The tests 44, 48 and 49 correspond to different profiles of potential temperature and water vapour mixing ratio and the tests 45, 46 and 47 correspond to different profiles of wind. When the profiles of potential temperature and water vapour mixing ratio were modified, the wind profiles of the

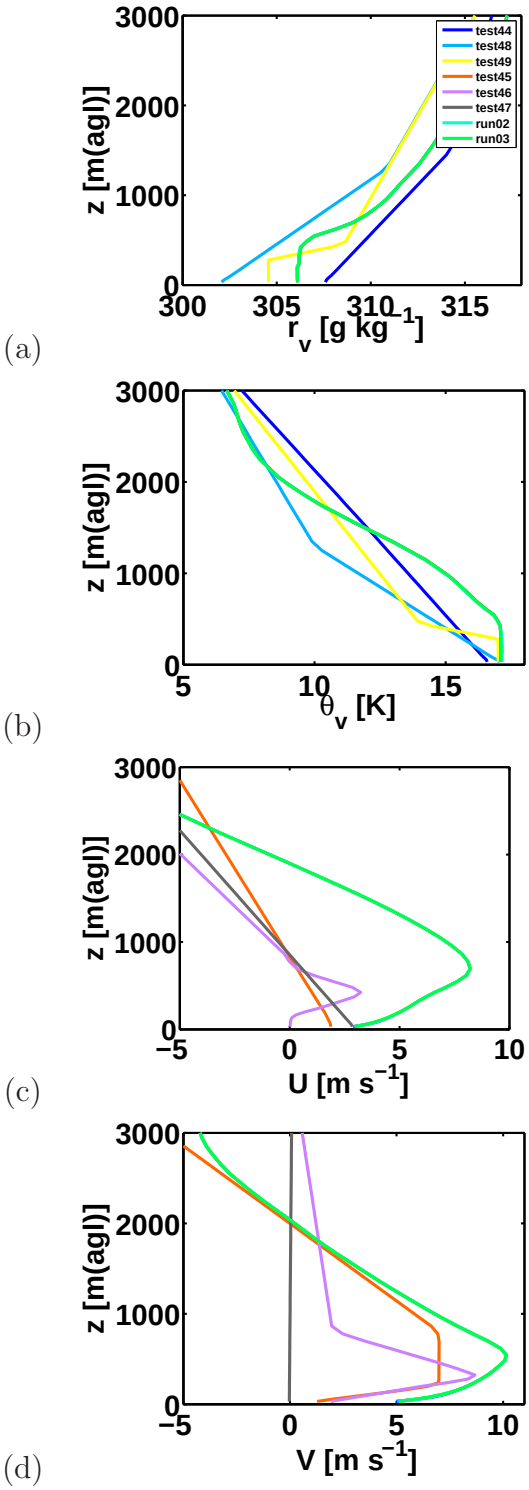

FIG. 7. *Vertical initial profiles of the 8 LES simulations of (a) the potential temperature, (b) water vapour mixing ratio, (c) zonal and (d) meridian wind components.*

reference simulation were used.

These 6 tests of sensitivity constitute, with the simulation of 5 June 2006, with and without advection, our set of sensitivity tests. They allow us to study the role of small scale processes within a typical Sahelian boundary layer.

a. Entrainment velocity analysis: ZOM vs FOM approximation

Aircraft observations in the area of study (Canut et al. 2010, Said et al. 2010) have often shown during this season values of β larger than the typical value of 0.2.

To quantify the growth of the PBL ($\frac{\partial Z_i}{\partial t}$), the entrainment velocity is used:

$$w_e = \frac{\partial Z_i}{\partial t} - w_h, \tag{3}$$

where w_h is the large-scale vertical velocity. w_h is usually small or has the same magnitude as w_e. w_e quantifies the engulfment of air from the free troposphere within the PBL. In the ZOM approach, it can be estimated by the ratio between the flux of a scalar quantity at the inversion and the jump in the scalar (θ, r_v or concentration of another trace gas) concentration (Lilly 1968, Faloona et al. 2005, Lenschow et al. (1999)):

$$w_e \simeq -\frac{\overline{ws}|_i}{\Delta s} \tag{4}$$

where 's' can be any scalar quantity, s= θ_v, r_v, ...

The entrainment velocity, w_e, was estimated from observations by using equations 2 and 3. Two soundings made at two different hours were used to obtain the boundary layer growth and w_e (equation 3, neglicting w_h) and aircraft observations provided the entrainment buoyancy fluxes in equation (4). By comparing these two estimations of w_e, we obtained smaller entrainment velocity when using the entrainment flux estimation by the ZOM. The main reason is that the ZOM model (equation 4) does not take into account the depth of the entrainment layer. The vertical structure observed should be better approximated by a first-order model in this region.

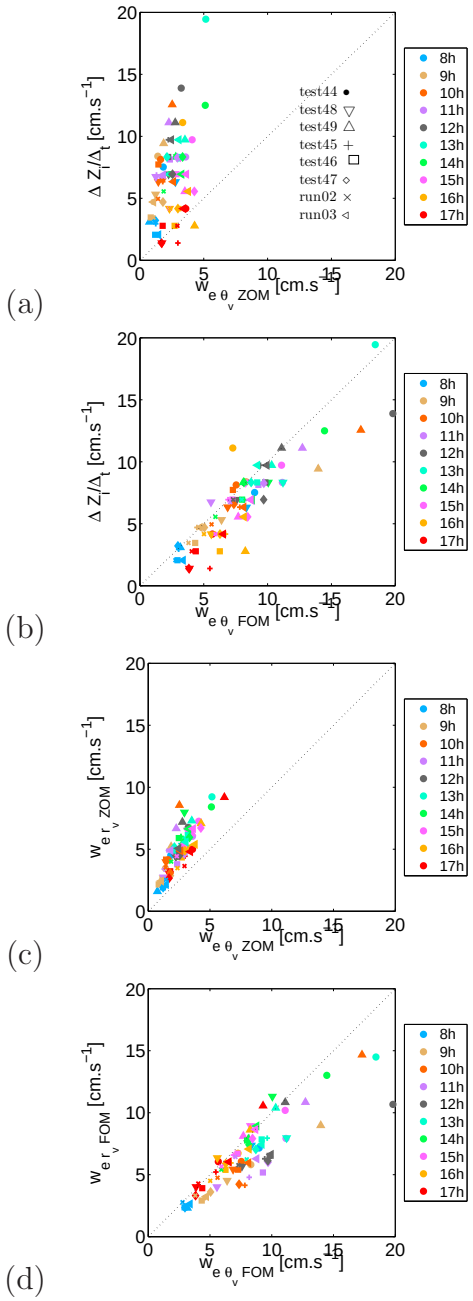

FIG. 8. *Comparison between $\frac{\Delta Z_i}{\Delta t}$ and w_e calculated with the potential temperature, based on (a) a ZOM model and (b) a FOM model. (c) and (d) compare w_e calculated with two different scalars (the virtual potential temperature and the vapour mixing ratio) respectively with a ZOM model and a FOM model.*

In the LES as in observations, the entrainment thickness zone is large, so the zero-order approximation is not correct. First Sullivan et al.

(1998), then Pino and Vilà-Guerau de Arellano (2008) used a parametrization of the entrainment velocity deduced from the FOM model. With this parametrization,

$$w_e \simeq \frac{\partial Zi}{\partial t} \simeq -\frac{\overline{w\theta_v}|_i}{\Delta\theta_v} + \frac{\delta}{\Delta\theta_v}\frac{\partial\theta_v}{\partial t} \simeq -\frac{\overline{wr_v}|_i}{\Delta r_v} + \frac{\delta}{\Delta r_v}\frac{\partial r_v}{\partial t}. \quad (5)$$

Thus, a connection term is added which takes account of the entrainment depth, and depends on the time evolution of the scalar. A much better comparison between $w_{e\theta_v}$, w_{er_v} and $\frac{\partial Zi}{\partial t}$ is obtained with equation 5 as shown in figure 8(a,b).

Figure 8 (c,d) shows the comparison between w_{er_v} and $w_{e\theta_v}$ obtained with the zero and the first order model. The correcting term from ZOM to FOM is smaller for w_{er_v} than for $w_{e\theta_v}$, because the profile of the water vapour mixing ratio is more similar to a zero-order jump model. However the FOM parameterization still improves the comparison.

The same parametrization for w_e was also used for all the studied flights despite the difficulty to determine $\frac{\partial\theta_v}{\partial t}$. For all the cases the first-order approximation improved the relation between $\frac{\Delta Zi}{\Delta t}$ and w_e (not shown).

As a conclusion, the FOM, by considering δ and the time evolution of the scalar parameters, seems to give a better framework for the estimates of the entrainment velocity. This result shows that the thickness of the entrainment layer and the temporal evolution of the scalar in the PBL are important parameters in the analysis of the entrainment processes.

b. *Role of the entrainment*

With the LES data and aircraft observations, we found the correlation between β and windshear in the entrainment zone, previously mentioned in several studies (Fedorovich and Conzemius (2008)). The windshear was calculated with

$$WS = (\Delta U^2 + \Delta V^2)^{\frac{1}{2}}$$

where ΔU and ΔV are the jump in zonal and meridian wind accross the entrainment zone. The entrainment rate increases (see figure 9) when the windshear increases. During the last hour of the simulation, β is poorly defined because the buoyancy flux at both PBL top and at surface are too small.

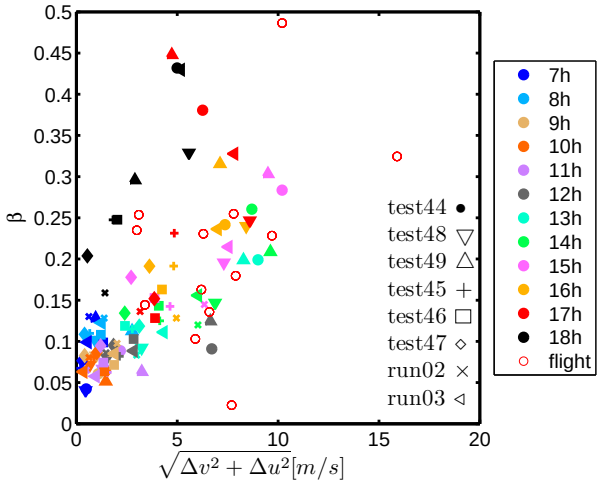

FIG. 9. *Comparison between the entrainment rate and the windshear at the PBL top*

Figure 10 represents the correlation between the entrainment velocity and the negative fluctuation in water vapour mixing ratio and in vertical velocity observed within the dry tongues. Large entrainment velocities are associated with large fluctuations of r_v and w. The minimum of w' is located in the middle of the PBL and the minimum of r'_v is located at the PBL top. The surface of the negative buoyancy flux, noted $B-$ in figure 1 is also an estimate of the engulfment of dry air into the PBL (Pino et al. (2006)). Figure 11 compares this area with the minimum of w' in the dry tongues. The most intense negative fluctuations of w yield large surface of the negative buoyancy flux.

c. *Tests of parameterization*

The complexity of the entrainment process makes it difficult to parameterize even in models which allow to resolve the characteristics of the bound-

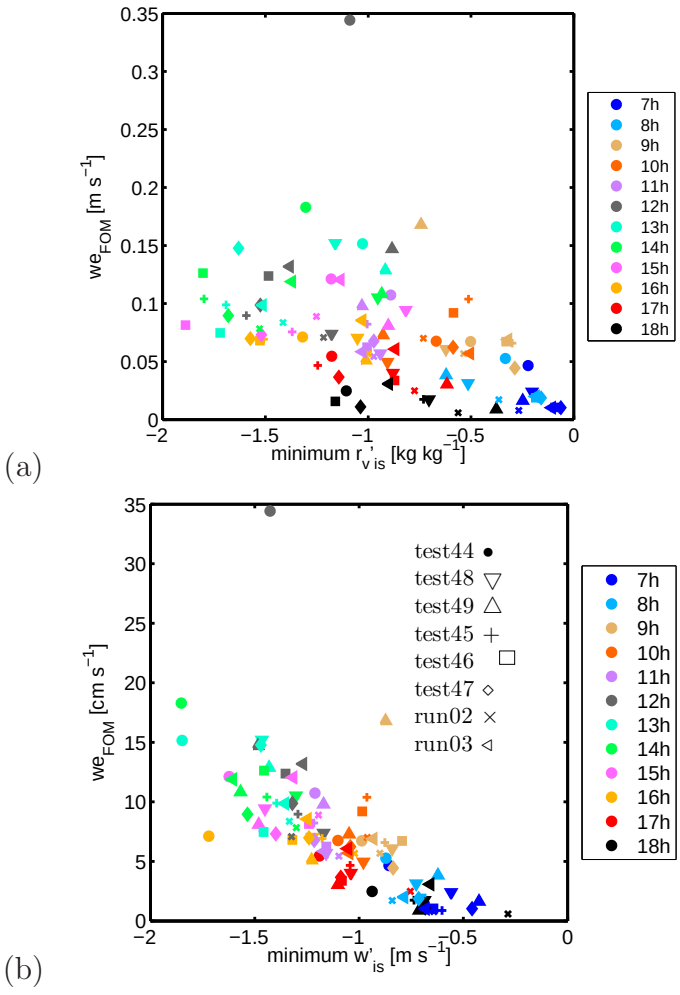

FIG. 10. *Comparison between the entrainement velocity and (a) the minimum of r'_v and (b) the minimum of w' in the dry intrusions*

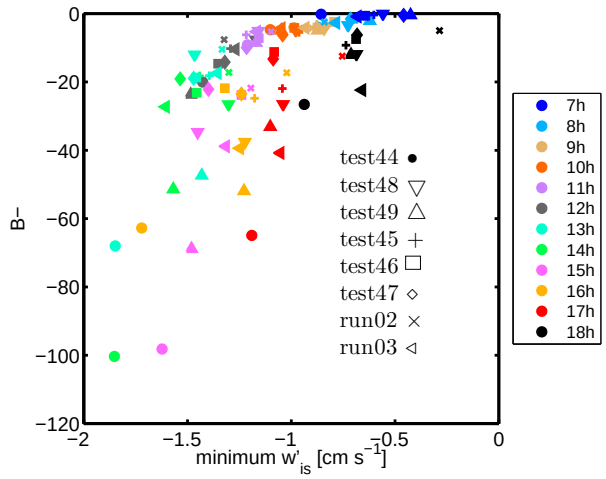

FIG. 11. *Comparison between the minimum of the vertical velocity fluctuation and the negative buoyancy flux surface*

ary layer and its interfaces. Pino et al. (2003) determined in a zero order model case, one parameterization of β depending on the windshear. Then Kim et al. (2003) and Pino et al. (2006) considered a first order model to improve the entrainment parameterization. In our case, it is very important to consider a first order model and consequently to include the entrainment zone in the process of the entrainment because the entrainment zone in this region is relatively thick. We evaluated the parameterizations of the rate of entrainment, of the entrainment velocity and of the entrainment zone thickness for a first order model.

To resolve the entrainment equations in a first order model, the thickness of the entrainment zone must be calculated. Several authors parameterized the entrainment zone with the Richardson number:

$$\frac{\delta}{Z_i} = b + \frac{a}{Ri} \qquad (6)$$

where $R_i = \frac{g}{\theta_v}\Delta\theta_v \frac{Z_i}{v_*^2}$ and $v_*^2 = w_*^2 + 4u_*^2 + 0.1(\Delta U^2 + \Delta V^2)$, u_* is the surface friction velocity and $w_* = \left(\frac{g}{\theta_v} Z_i \overline{w'\theta'_v|_0}\right)^{1/3}$ is the convective velocity.

Figure 12 compares the parameterized entrainment zone thickness with δ calculated directly with the LES flux profile. By using the same constants as in Pino et al. (2006), a=1.12 and b=0.08, we obtained a satisfying correlation.

We remind here that under free convection conditions the most common way of estimating the buoyancy flux at Z_i is to consider that it is 20% of the buoyancy flux at the surface.

This estimation of flux at the PBL top is discussed in numerous studies (Moeng and Sullivan (1994); Sullivan et al. (1998); Pino et al. (2003) and many others), which agree to say that this fraction of the surface flux can vary according to time and boundary layer characteristics. Our experimental and numerical studies confirm this re-

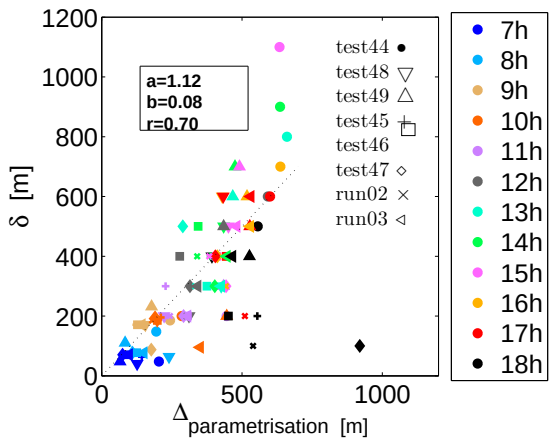

FIG. 12. *Comparison of the depth of the entrainment zone calculated with the parameterization (Pino et al. (2006)) and directly estimated with the buoyancy flux profile. The coefficients a and b correspond to the coefficients used in equation (6) and r is the correlation coefficient.*

sult.

We tested the parameterization of β as well as that of w_e. We used the equations proposed by Pino et al. (2006), Kim et al. (2006) and Sun and Xu (2009) based on the vertically integrated turbulent kinetic energy budget in the sheared CBL:

$$\beta_{FOM} = \left(A_1 \frac{1}{1+\frac{\delta}{Z_i}} + A_2 \left(\frac{u_*}{v_*}\right)^3 + A_3 \frac{\delta}{4Z_i + 2\delta} \right.$$

$$\left. \left[\frac{u_*^2 \Delta U}{w_*'^3} + \frac{\overline{\theta_v} \Delta U^2}{g\,(Z_i+\delta)\,(\Delta\theta_v - 0.5\gamma_\theta \delta)} \right] \right) \times$$

$$\left[1 - \frac{\overline{\theta_v} \Delta U^2}{2g\,(\Delta\theta_v - 0.5\gamma_\theta\delta)\,(Z_i+\delta)} A_3 \right]^{-1} \qquad (7)$$

$$w_{e_{FOM}} = \frac{\partial Z_i}{\partial t}|_{FOM} = -\frac{\delta - (2h+\delta)\beta_{FOM}}{h(2\Delta\theta_{vFOM} - \gamma\delta)} \overline{w'\theta_v'}|_0 \qquad (8)$$

This parameterization takes into account the wind-shear across the inversion layer (by using ΔU and v_*) and the shear in the surface layer (by using u_* and v_*). We tested the values provided by Pino et al. (2006), since $A_1 = 0.2$ is consistent with the classical closure value for a CBL with negligible shear, and $A_2 = 0.26$ agrees with the argument that most of the TKE produced at the surface dissipates locally. Kim et al. (2006) and Pino et al. (2006) used $A_3 = 1.44$ in this parameterization of entrainment heat flux. This value implies that about 70% of the inversion layer shear produced TKE is available for the enhancement of entrainment. The study from Conzemius and Fedorovich (2006) and Sun and Yuan (2008) suggests that the coefficient A_3 needs to be ajusted.

Figure 13 compares, for w_e and β, the parameterized values in the LES to the direct values derived respectively from the growth of the PBL $\frac{\partial Z_i}{\partial t}$ or the flux profile. The largest entrainment velocity values as well as most flux ratio values are over-estimated by the parameterization which shows that parameterizations still need to be refined. Figure 14 shows the same comparison as in figure 13(b), but using A_3=1. With this value the parameterization seems to give a better results.

5. Conclusions

The sensivity tests based on the observations made on 5 June 2006 allowed us to study the role of some key variables in the entrainment processes. The tests presented a large range of conditions with a wind jump between the PBL and the free troposphere varying between 0 and 13 m s^{-1}. The numerical study confirms the importance to consider a first order model to estimate the entrainment processes for the studied cases. Nevertheless this study shows the limitation of this model for large entrainment values($w_e > 10 m s^{-1}$).

The tests enable us to evaluate the parameterizations used in the literature in more realistic conditions, i.e. comparing with observations. The parameterization of the entrainment zone depth fits well the simulated values with the Richardson

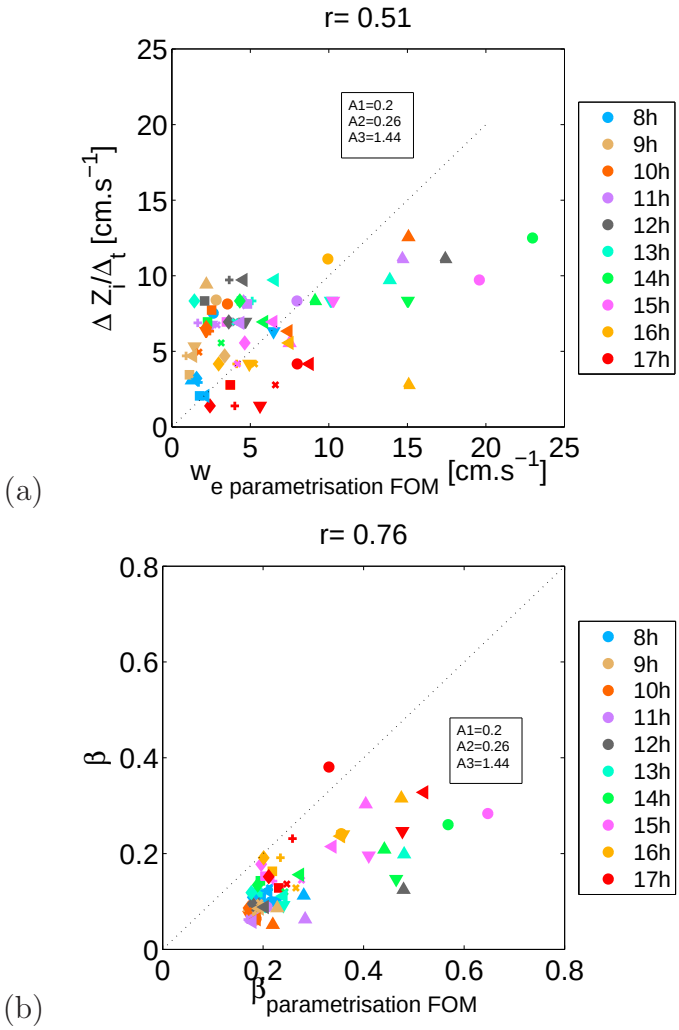

FIG. 13. *Comparison between (a) the PBL growth rate and the parametrized entrainment velocity and (b) the parametrized entrainment rate and the entrainment rate obtained by the buoyancy flux, using* $A_3 = 1.44$.

number method. However, the parameterization of the entrainment velocity and rate proposed by Pino et al. (2006) is not really satisfying for our set of data, but improved with $A_3 = 1$. This shows that the existing parametrizations are not universal and still need more confrontation with the observations.

Acknowledgments.

The research of D. Pino was partially funded by the Spanish Ministry of Science and Innovation

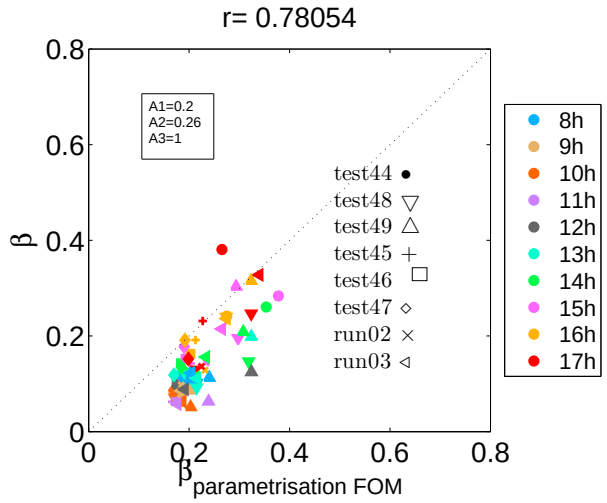

FIG. 14. *Comparison between the parametrized entrainment rate and the entrainment rate obtained by the buoyancy flux, using* $A_3 = 1$.

(MICINN, CGL2009-08609) and by the European project INTERREG FLUXPYR EFA 34/08.

REFERENCES

Agusti-Panareda, A., et al., 2010: The ecmwf reanalysis for the amma observational campaign. *Quart. J. Roy. Meteorol. Soc.*, **submitted**.

Betts, A. K., 1974: Reply to comment on the paper 'non-precipitating cumulus convection and its parameterization'. *Quart. J. Roy. Meteorol. Soc.*, **100**, 469–471.

Canut, G., M. Lothon, F. Lohou, and F. Said, 2010: Observation of entrainment at the interface between monsoon flow and Saharan Air Layer. *Quart. J. Roy. Meteorol. Soc.*, **136**, 34–46.

Conzemius, R. J. and E. Fedorovich, 2006: Dynamics of sheared convective boundary layer entrainment. textscPart II: Evaluation of bulk model predictions of entrainment flux. *J. Atmos. Sci.*, **63**, 1179–1199.

Couvreux, F., F. Guichard, J. L. Redelsperger, C. Kiemle, V. Masson, J. P. Lafore, and C. Flamant, 2005: Water-vapour variability within a convective boundary-layer assessed by large-eddy simulations and ihop-2002 observations. *Quart. J. Roy. Meteorol. Soc.*, **131**, 2665–2693.

Couvreux, F., F. Guichard, J. L. Redelsperger, and V. Masson, 2007: Negative water vapour skewness and dry tongues in the convective boundary layer: observations and LES budget analysis. *Boundary-Layer Meteorol.*, **123**, 269–294.

Cuxart, J., P. Bougeault, and J. L. Redelsperger, 2000: A turbulence scheme allowing for mesoscale and large-eddy simulations. *Quart. J. Roy. Meteorol. Soc.*, **26**, 1–30.

Faloona, I., et al., 2005: Observations of entrainment in eastern pacific marine stratocumulus using three conserved scalars. *J. Atmos. Sci*, **62**, 3268–3285.

Fedorovich, E. and R. Conzemius, 2008: Effects of wind shear on the atmospheric convective boundary-layer structure and evolution. *Acta Geophysica*, **56**, 114–141.

Garratt, J. R., 1992: *The atmospheric boundary layer*. Cambridge atmospheric and space science series.

Grossman, R. L. and G. Nimal, 1995: Moisture flux and mixing processes in the daytime continental convective boundary layer. *Journal of Geophysical Research*, **100**, 25,665–25,674.

Kim, S., S. Park, and C. H. Moeng, 2003: Entrainment processes in the convective boundary layer with varying wind shear. *Boundary-Layer Meteorol.*, **108**, 221–245.

Kim, S.-W., S.-U. Park, D. Pino, and J. Vilà-Guerau de Arellano, 2006: Parameterization of entrainment in a sheared convective boundary layer using a first-order jump model. *Boundary-Layer Meteorol.*, **120**, 445–475.

Lafore, J. P., et al., 1998: The Meso-NH atmospheric simulation system. Part I: Adiabatic formulation and control simulations. *Annales Geophysicae*, **109**, 16–90.

Lenschow, D. H., P. B. Krummel, and S. T. Siems, 1999: Measuring entrainment, divergence and vorticity on the mesoscale from aircraft. *J. Atmos. Oceanic Technol.*, **16**, 1384–1400.

Lilly, D. K., 1968: Models of cloudy-topped mixed layers under a strong inversion. *Quart. J. Roy. Meteorol. Soc.*, **94**, 292–309.

Lohou, F., F. Said, M. Lothon, P. Durand, and D. Serç a, 2010: Impact of the boundary-layer processes on surface turbulence characteristics in the frame of the west african monsoon. *Boundary Layer Meteorol.*, **136**, 1–23.

Moeng, C. H. and P. Sullivan, 1994: A large-eddy simulation model for the study of planetary boundary layer turbulence. *J. Atmos. Sci.*, **51**, 999–1022.

Pino, D. and J. Vilà-Guerau de Arellano, 2008: Effects of shear in the convective boundary layer: analysis of the turbulent kinetic energy budget. *Acta Geo.*, **56**, 167–193.

Pino, D., J. Vila-Guerau De Arellano, and P. G. Duynkerke, 2003: The contribution of shear to the evolution of a convective boundary layer. *J. Atmos. Sci.*, **60**, 1913–1926.

Pino, D., J. Vilà-Guerau de Arellano, and S.-W. Kim, 2006: Representing sheared convective boundary layer zero- and first-order-jump mixed-layer models: Large-eddy simulation verification. *J. Appl. Meterol. Clim.*, **45**, 1224–1243.

Redelsperger, J. L. and G. Sommeria, 1982: Method of representing the turbulence at scales inferior to the grid in a three-dimensional model of cloud convecion. *Boundary-Layer Meteorol.*, **21**, 509–530.

Said, G., F. Canut, M. Durand, P. Lothon, and F. Lohou, 2010: Seasonal evolution of boundary-layer turbulence measured by aircraft during the AMMA 2006 special observation period. *Quart. J. Roy. Meteorol. Soc.*, **136**, 47–65.

Stull, R. B., 1976: The energetics of entrainment across a density interface. *J. Atmos. Sci.*, **33**, 1260–1267.

Sullivan, P. P., C.-H. Moeng, B. Stevens, D. H. Lenschow, and S. D. Mayor, 1998: Structure of the entrainment zone capping the convective atmospheric boundary layer. *Quart. J. Roy. Meteorol. Soc.*, **55**, 3042–3064.

Sun, J. and Q. Xu, 2009: Parameterization of sheared convective entrainment in the first-order jump model: Evaluation through large-eddy simulation. *Boundary-Layer Meteorol.*, **132**, 279–288.

Sun, J. and W. Yuan, 2008: Effect of the entrainment flux ratio on the relationship between entrainment rate and convective Richardson number. *Boundary-Layer Meteorol.*, **126**, 237–247.

Tennekes, H., 1973: A model for the dynamics of the inversion above a convective boundary layer. *J. Atmos. Sci.*, **30**, 538–567.

Turner, D., E. Wagner, V. Wulfmeyer, S. Pal, and K. Larry, 2010: Raman lidar observations of water vapor mixing ratio turbulence profiles in the convective boundary layer. *oral presentaion, ISARS.*

Van Zanten, M. C., P. Duynkerke, and J. Cuijpers, 1999: Entrainment parameterization in convective boundary layers. *J. Atmos. Sci.*, **56**, 813–828.